Theoretical analysis of the ECH effect on the energetic particle driven modes stability in Heliotron J

J. Varela[1], K. Nagasaki[2], K. Nagaoka[3], S. Yamamoto[4], D. Spong[5], L. Garcia[1], A. Cappa[6] and K.Y. Watanabe[3]

[1] *Universidad Carlos III de Madrid, 28911 Leganes, Madrid, Spain*

[2] *Institute of Advanced Energy, Kyoto University, Uji, Japan*

[3] *National Institute for Fusion Science, NINS, Toki, 509-5292, Japan*

[4] *National Institute for Quantum and Radiological Science and Technology, Naka Fusion Institute, Naka-shi, Ibaraki-ken 311-0193 Japan*

[5] *Oak Ridge National Laboratory, Oak Ridge, Tennessee 37831-8071*

[6] *Laboratorio Nacional de Fusion CIEMAT, Madrid, Spain*

Abstract

The aim of the study is to analyze the stability of the Energetic Particle Modes (EPM) and Alfven Eigenmodes (AE) in Heliotron J if the electron cyclotron heating (ECH) is applied. The analysis is performed using the code FAR3d [1]. The simulations indicate that the modes with the largest growth rate in the Heliotron J high bumpiness (HB) and medium bumpiness (MB) magnetic configurations are $n/m = 1/2$ and $2/4$ global AE (GAE). On the other hand, the simulations for the low bumpiness (LB) configurations show the destabilization of $1/2$ EPM and $2/4$ GAE. The simulations for LB configuration show a dominant stabilizing effect of the continuum damping with respect to the increase of the EP β as T_e increases. On the other hand, the simulations for the HB and MB configurations indicate that the further destabilization of the AE/EPM caused by the increase of the EP β with T_e is larger with respect to the stabilizing effect of the continuum damping.

Introduction

The application of ECH in Heliotron J plasma leads to the stabilization or the further destabilization of the AE/EPM according to the device configuration [2, 3, 4]. The AE/EPM are stabilized in the low bumpiness (LB)configuration although further destabilized in the high bumpiness (HB) and medium bumpiness (MB) configurations [5]. The complexity of the ECH effect on the AE/EPM stability is linked to the combined variation of several plasma parameters as the EP β, EP resonance properties, plasma resistivity, continuum damping, thermal plasma β, electron-ion Landau damping between others. Using FAR3d code a set of parametric studies are performed identifying the dominant trends affecting the AE/EPM stability.

Numerical scheme

The FAR3d code solves the linear evolution of the thermal plasma (poloidal flux, total pressure, toroidal component of the vorticity and thermal parallel velocity) coupled with the equations of the EP density and parallel velocity moments. The present model was already used to study the AE stability in several magnetic confinement fusion devices [6, 7], indicating reasonable agreement with the observations. The reader can find more details of the numerical model in these references. Three fixed boundary results from the VMEC equilibrium code are used for LB, MB and HB configurations of Heliotron J. Figure 1 indicates the main profiles of the models. The magnetic field at the magnetic axis is 1.25 T. The magnetic Lundquist number is assumed $S = 5 \cdot 10^6$. The dynamic toroidal modes (n) in the simulations are the $n = 1$ and 2 with the dynamic poloidal modes (m) $m = [1,3]$ and $[2,5]$, respectively, covering the main resonant rational surfaces. The equilibrium modes ($n = 0$) are $m = [0,14]$.

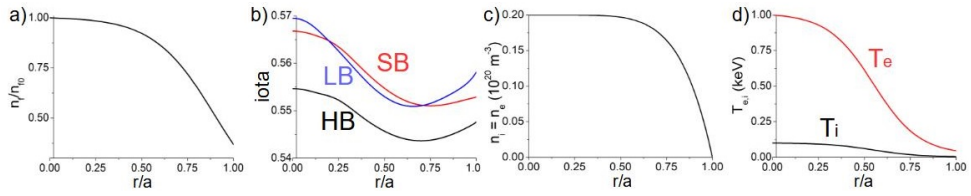

Figure 1: Main profiles. (a) EP density (b) iota (c) thermal electron and ion density, (d) thermal electron and ion temperature

Low bumpiness configuration

Figure 2 (panels a and b) indicates that a stronger ECH injection leads to a smaller AE/EPM activity. FAR3d simulations identifies instabilities with frequency, dominant modes and eigenfunction radial location consistent with the experiment (panels c and d). AE/EPM are further destabilized as the EP β (panels e and f) and EP thermalization temperature (panels g and h) increase. For the thermal β values consistent with the experiment $1/2$ EPM and $2/4$ GAE growth rate decrease as thermal β increases (panels i and j). The continuum damping effect is dominant as T_e increases (panels k and m).

High bumpiness configuration

Figure 3 (panels a and b) indicates that a stronger ECH injection leads to a stronger activity of the instabilitis in the frequency range of the 125 and 175 kHz. FAR3d simulations show instabilities with frequency ranges similar to the experiment (panels c and g). The dominant instabilities are $1/2$ and $2/4$ BAEs, weakly stabilized by the continuum damping effect (panels m and n). AE/EPM growth rate increases as the EP β increases (panels h and i) and decreases

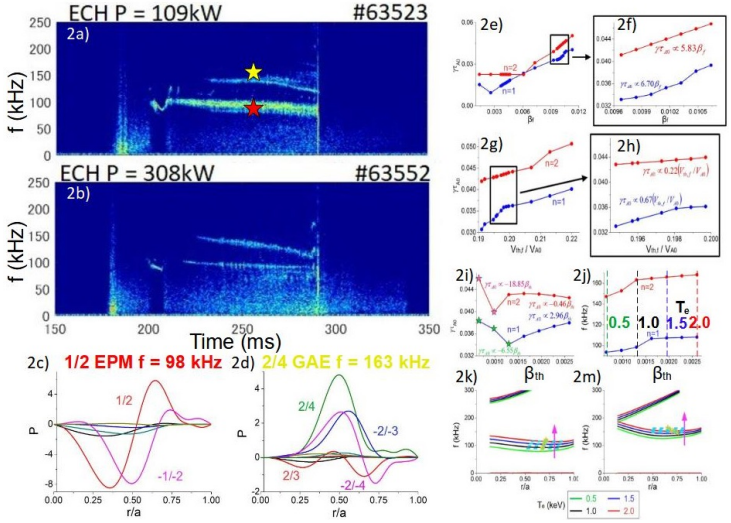

Figure 2: Magnetic spectrogram of discharges with ECH power injection of (a) 109 kW and (b) 308 kW. Pressure eigenfunction of (c) $1/2$ EPM and (d) $2/4$ GAE. AE/EPM growth rate versus (e) EP β and (g) $V_{th,f}/V_{A0}$. Regression of AE/EPM growth rate versus (f) EP β and (h) $V_{th,f}/V_{A0}$. AE/EPM (i) growth rate and (j) frequency versus thermal β. Alfven gaps of the (k) $n = 1$ and (m) $n = 2$ modes (frequency range and radial width of the AE/EPM included).

as the thermal β increases (panels j and k). although the destabilizing trend of the EP β is dominant.

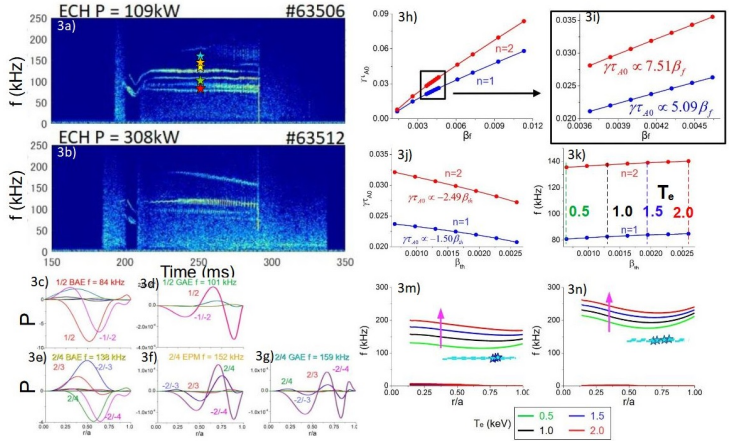

Figure 3: Magnetic spectrogram of discharges with ECH power injection of (a) 109 kW and (b) 308 kW. Pressure eigenfunction of (c) $1/2$ BAE, (d) $1/2$ GAE, (e) $2/4$ BAE, (f) $2/4$ EPM and (g) $2/4$ GAE. (h) AE/EPM growth rate versus EP β. (i) Regression of AE/EPM growth rate versus EP β. AE/EPM (j) growth rate and (k) frequency versus thermal β. Alfven gaps of the (m) $n = 1$ and (n) $n = 2$ modes (frequency range and radial width of the AE/EPM included).

Medium bumpiness configuration

Figure 4 (panels a and b) indicates the further destabilization of instabilities in the frequency range of 100 and 120 kHz. FAR3d simulations show instabilities with a frequency consistent with the experiment (panels c and g). The dominant instabilities are $1/2$ GAE and $2/3$ EPM (panels m and n). AE/EPM are further destabilized as the EP β increases (panels h and i) although the growth rate decreases as the thermal β increases (panels j and k). EP β destabilizing effect is dominant.

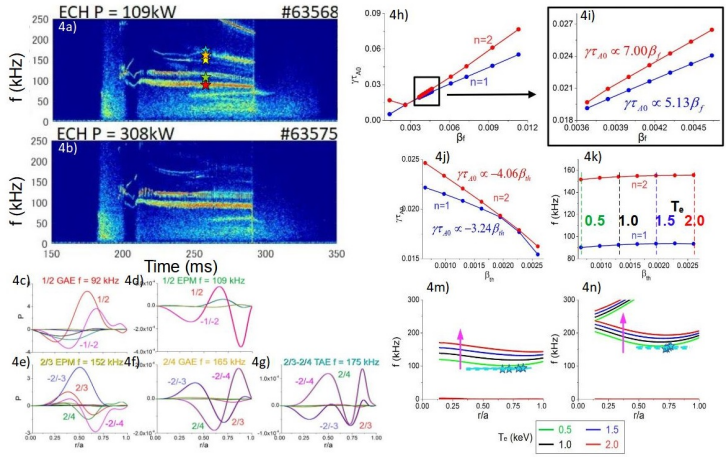

Figure 4: Magnetic spectrogram of discharges with ECH power injection of (a) 109 kW and (b) 308 kW. Pressure eigenfunction of (c) $1/2$ GAE, (d) $1/2$ EPM, (e) $2/3$ EPM, (f) $2/4$ GAE and (g) $2/3-2/4$ TAE. (h) AE/EPM growth rate versus EP β. (i) Regression of AE/EPM growth rate versus EP β. AE/EPM (j) growth rate and (k) frequency versus thermal β. Alfven gaps of the (m) $n=1$ and (n) $n=2$ modes (frequency range and radial width of the AE/EPM included).

This work is supported by the projects 2019-T1/AMB-13648 (Comunidad de Madrid), NIFS Collaborative Research Program NIFS08KAOR010, NFIS10KUHL030, NIFS07KLPH004 and "PLADyS" JSPS Core-to-Core Program, A. Advanced Research Networks and by multiannual agreement with UC3M (“Excelencia para el Profesorado Universitario” - EPUC3M14) - Fifth regional research plan 2016-2020 Comunidad de Madrid (Spain).

References

[1] J. Varela et al *Nucl. Fusion*, **57**, 046018 (2017).

[2] K. Nagasaki et al *Nucl. Fusion*, **53**, 113041 (2013).

[3] S. Yamamoto et al *Nucl. Fusion*, **57**, 126065 (2017).

[4] S. Yamamoto et al *Nucl. Fusion*, **60**, 066018 (2020).

[5] K. Nagasaki et al *28th IAEA Fusion Energy Conference*, **EX/P6-34** (2021).

[6] J. Varela et al *Nucl. Fusion*, **60**, 112015 (2020).

[7] A. Cappa et al *Nucl. Fusion*, **61**, 066019 (2021).